

# COMPREHENSIVE FULLY AUTOMATED LEFT-VENTRICULAR EJECTION AND CONTRACTILITY ANALYSIS

*G. Angus-Barker and J. Kar*

Department of Mechanical Engineering, University of South Alabama, Mobile, Alabama, USA  
gva1521@jagmail.southalabama.edu

**Abstract**— This study presents a novel fully-automated mechanism for MRI-based profiling of left-ventricular (LV) chamber quantities and mechanical properties (3D strains, twist and torsion) for the cardiac cycle. Comprehensive LV contractile analysis was conducted by extending a validated semi-automated methodology for spatiotemporal myocardial boundary detection, whose underlying algorithm consists of a multi-threshold image quantization process and 3D phase-unwrapping of complex MRI images acquired with the Displacement Encoding with Stimulated Echoes (DENSE) sequence. Demonstrating this tool's feasibility included cross-validating computations of LV torsion using two different techniques (a boundary deformation-based and a strain-based one) and by showing how torsional mechanics correlate with ejection fraction (EF) in the phase following isovolumetric contraction. The quantization and displacement results acquired in all 2D partitions at subsequent timeframes lead to 3D LV reconstructions and determination of contractile parameters in N=15 healthy subjects. Statistical tests consisted of Bland Altman analysis of results from the two torsional computations and establishing correlations between EF and torsion. Bland Altman biases and limits of agreement between the two methods for regional torsions were  $0.20 \pm 2.4^\circ$  and  $0.19 \pm 1.97^\circ$  for the mid-ventricular and basal sub-regions (both relative to apex), respectively. Strong Pearson's correlations found between torsion and EF were  $R^2 = 0.80$  ( $p < 0.001$ ) and  $R^2 = 0.82$  ( $p < 0.001$ ) for the mid-ventricular and basal segments, respectively. The results from the statistical analysis demonstrate that the methodology developed for comprehensive cardiac contractility analysis can be used reliably in healthy subjects, with a potential for extending application in diagnosing cardiac dysfunction.

## I. INTRODUCTION

This study was conducted to investigate the feasibility of a fully automated, single-scan, MRI-based methodology for assessing full left-ventricular (LV) function (strain-based contraction and chamber quantifications such as, chamber diameters (CD), ejection volumes (EV) and ejection fraction (EF)) between the end-diastole and end-systole phase of the cardiac cycle. The rapid processing capabilities of this tool involving the computation of a wide range of contractile parameters, (including EF and 3D myocardial strains) spanning the cardiac cycle ejection phase can be highly advantageous for clinical diagnosis applications. Additionally, this study specifically targets the computation of LV shear strains, twist and torsion due to the prevailing belief in the medical community being that torsion which parameterizes the wringing motion of the heart's myofibers during ejection can indicate cardiac

dysfunction [1-4]. A novel and fast 3D automated methodology was used to achieve the rapid processing that tracks LV contractility and boundary motion through phase unwrapping of MRI data recorded with the navigator-gated spiral Displacement Encoding with Stimulated Echoes (DENSE) sequence [5-9]. The displacement-based boundary search is further reinforced with a histogram-based thresholding approach called Otsu's method which identifies myocardial tissue according to quantization indices related to discrete ranges of pixel intensities [10, 11]. Additionally, presented here is the first 3D, automated strain analysis and surface strain map generation methodology that applies the above automated LV boundary detection and spatiotemporal displacements analysis processes [12, 13].

## II. EXPERIMENTAL DESIGN

### A. Human Subject Recruitments

A total of 15 healthy (normal) subjects (eight females and seven males) were imaged in a 1.5 Tesla Espree (Siemens, Erlangen, Germany) MRI scanner using the navigator-gated 3D Spiral DENSE sequence [8, 9]. All subjects signed informed consents in accordance with the university's Institutional Review Board (IRB) guidelines where they declared the absence of any form of cardiac disease.

### B. DENSE Acquisition and Protocols

Navigator-gated 3D DENSE data were acquired with displacement encoding applied in two orthogonal in-plane directions and one through plane direction [5, 6, 9, 14]. A flexible, anterior 6-channel body matrix RF coil (Siemens Healthcare, Erlanger, Germany) and the table-mounted spine matrix RF coil were used for receiving signals. Typical imaging parameters included field of view (FOV) of  $380 \times 380$  mm<sup>2</sup>, echo time (TE) of 1.04 ms, repetition time (TR) of 15 ms, matrix size of  $128 \times 128 \times 19$ ,  $2.97 \times 2.97 \times 5$  mm<sup>3</sup> voxel size, 21 cardiac phases, encoding frequency of 0.06 cycles/mm, simple 4-point encoding and 3-point phase cycling for artifact suppression [8, 9]. The number of navigator-accepted heartbeats to complete a single partition in 3D is 36 heartbeats given that three are needed to acquire a complete set of spirals for a single displacement encoding direction and a single phase cycling point [9]. Continuous monitoring of heart rates (HR) and blood pressures (BP)

was conducted during the scans for all subjects.

### C. Image Quantization

The first step in this automated process is identification of the left-ventricular boundary contours in each short axis slice at a reference timeframe with the operator selecting an ellipsoidal region of interest (ROI) in the most basal short-axis slice at end-diastole and followed by propagating that ROI to all slice positions ending at the apex. The LV boundaries and intramural tissue are then identified when a threshold image is formed with a distinct profile of the short-axis using a non-uniform quantization scheme based on image histogram bins (with the most commonly occurring pixel intensities) called Otsu's Method [10, 11]. In its most basic form, Otsu algorithm separates two classes of pixels based on a bi-modal histogram and calculates the optimum threshold separating the two classes such that their inter-class variance is maximal [10, 11]. In the multi-modal system Otsu's method maximizes the inter-class variance,  $\sigma_b^2$ , in an image of M number of pixel bins or classes with M-1 thresholds,  $(t_1, t_2, \dots, t_{M-1})$  [10]. This maximizing interclass variance is given by,

$$\sigma_b^2 = \sum_{k=1}^M \omega_k (\mu_k - \mu_T)^2 \quad (1)$$

$$\mu_k = \frac{\sum_{i \in C_k} p_i}{\omega(k)} \quad (2)$$

$$\omega_k = \sum_{i \in C_k} p_i \quad (3)$$

where  $p_i$  indicates the individual pixel intensity,  $\omega_k$  is the zero-order cumulative moment,  $\mu_k$  is mean intensity of the pixels in each class, and  $\mu_T$  is the cumulative mean for the entire image of the kth class  $C_k$ . The effective number of thresholds (number of classes selected) is determined by the effectiveness metric (EM), and an example of a bi-level thresholded quantization scheme in a short-axis slice is shown in Figure 1. EM for each image in the entire stack can be computed by iterating through a range of numbers of threshold bins and their computation details as given in a previous publication by one of the current authors [7].

### D. Boundary Detection with Displacement Encoding

In general, assessing cardiac kinematics requires the influence of soft tissue deformation on both amplitude and phase signals. Sequences such as DENSE accomplish the above through well-established magnetic field gradients/Fourier Transform method phenomenon called the pulsed gradient stimulated echo (PGSTE) which incorporates motion encoding by employing a pair of pulsed field gradients [15]. Hence, DENSE employs the PGSTE technique to encode tissue displacement in the phases of stimulated echoes, in a frame-by-frame

pixelwise incremental fashion from which semi-automated myocardial boundary motion is finally derived. Detailed descriptions for phase-to-displacement conversions with pixelwise phase unwrapping can be found in several previous publications, including the studies in DENSE-based strain validation [5, 6, 9, 13, 16]. As a final step, the raw displacement data is refined using temporal fitting of each pixel's trajectory with a 5<sup>th</sup> order Fourier basis functions [6, 9, 14, 16]. Implementing the strategy for detecting a boundary point's location began by a radial search for peaks in the pixel-based threshold gradients computed from the quantized images. With pixel-based intensity gradients computed in a radial direction, points on a starting bounding ellipse can be moved across the LV myocardium to detect peaks via the abrupt changes in intensities as shown in Figure 1. While edge detection based on searching gradients related to the differences in intensity of image pixels is a common mechanism, this study is unique in combining the unwrapped displacement vectors toward precisely

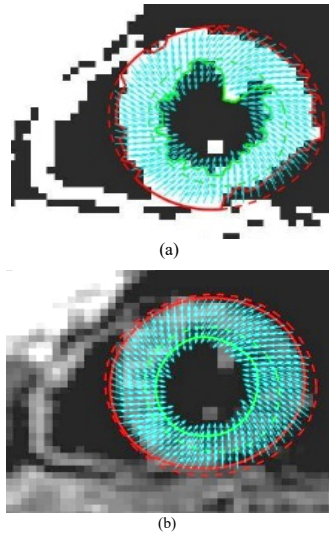


**Figure 1.** (a) Initial boundaries detected using Otsu's Method (2 quantization classes) and (b) Final boundaries with displacement and LOESS fitting based refinement.

tracking the relocation of a boundary point between end-diastole and end-systole. Final smoothing of boundary contours was conducted by fitting a non-parametric

regression, LOcal regrESSion (LOESS), curve to the new boundary points at each timeframe. The smoothing was then controlled by implementing a shape constraint based on minimizing an error function, of which further details are given in previous publications by one of the co-authors [17, 18].

Following the generation of boundaries for all partitions and timeframes using the above techniques as well as 3D reconstruction, well-established formulas provided in gold standard MRI studies generated measurements for chamber quantities at each timeframe for parameters like LV wall thickness, chamber diameters, end-diastolic volume (EDV), end-systolic volume (ESV) and EF [19].

### E. Meshfree Strain Analysis

Three-dimensional strain tensors were computed using RPIM at each voxel in patient-specific, MRI-based reconstructed 3D grid geometries. RPIM is a numerical analysis technique based on the Galerkin weak form that uses radial basis functions (RBF) as 3D meshfree shape functions and facilitates fast multidimensional computation of Lagrangian strains [14, 16, 20-22]. Since RPIM shape functions have the Kronecker delta functions property, essential boundary conditions are simply enforced, as otherwise done in finite element analysis (FEA). Hence, combining the advantages of DENSE with RPIM provides fast and effective 4D spatiotemporal analysis of strain, readily computed at a given voxel, without the tedium of keeping track of tagged data or remeshing interventions that otherwise prolong modelling time in traditional FEA [6, 8]. Extensive descriptions of both RPIM and its use in computing 3D LV strains is outlined in previous literature which, in particular, details the use of the Multiquadrics (MQ) as RBF shape function that ensures  $C^1$  continuity [14, 16, 20-22]. The final generation of LV phase unwrapped 3D displacements and segmentation prior to generation of strains is shown in Figure 2.

Our emphasis in the past has been to compute normal strains with RPIM to validate our automated strain analysis algorithm, and particularly given that normal longitudinal strain is the prevalent method for showing cardiac dysfunction. However, the emerging trend within the medical community is in investigating torsion (and shear strains) as indicators of cardiac dysfunction, where torsion is essentially the parameter determining the wringing motion of the heart's myofibers during ejection [1-4]. Hence, it is very important to understand how the contraction-relaxation behavior of the spiraling myofibers represents the twisting and torsion in the LV. There are several definitions for LV torsion including specifying it as the relative twist angle between basal and apical rotations, dividing twist by the length of the ventricle and others, including one that describes torsion as the circumferential-longitudinal shear angle ( $\alpha_{CL}$ ) [23-25]. This study will use the definition of torsion as  $\alpha_{CL}$ , which is a form that is comparable between hearts of

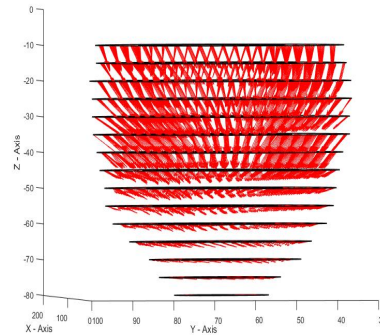


**Figure 2.** Three-dimensional displacement vectors and boundaries which contribute to the computation of the 9-element strain tensor at each grid point.

different sizes and directly relates fiber orientation to the process of wall motion, given by [25],

$$\alpha_{CL} = \sin^{-1} \left( \frac{2E_{CL}}{\sqrt{1 + 2E_{CC}} \sqrt{1 + 2E_{LL}}} \right) \quad (4)$$

where  $E_{CC}$  = circumferential strain,  $E_{LL}$  = longitudinal and  $E_{CL}$  = circumferential-longitudinal strain. To validate the method for computing torsion, a second methodology for computing it is given by [1],

$$\alpha_T = \frac{(\varphi_{base} - \varphi_{apex})(\rho_{base} + \rho_{apex})}{2D} \quad (5)$$

where  $\varphi$  is the angle of twist,  $\rho$  is the diameter and  $D$  is the distance between apex to base. It is noted that Eqn. (5) relies on our pre-validated method for semi-automated computing of boundary contours and automated computing of displacement vectors for twist.

## III. RESULTS AND ANALYSIS

**Table 1. Systolic and Diastolic Chamber Quantifications**

Parameter	Diastolic	Systolic
Diameter Basal (cm)	5.4 ± 0.6	3.4 ± 0.6
Diameter Mid (cm)	4.6 ± 0.6	2.8 ± 0.6
Diameter Apical (cm)	3.6 ± 0.4	2.4 ± 0.4
EF Basal	0.1 ± 0.1	0.6 ± 0.1
EF Mid	0.0 ± 0.1	0.6 ± 0.0
EF Apical	0.0 ± 0.1	0.6 ± 0.1
CV Basal (cm <sup>3</sup> )	68.7 ± 16.7	27.2 ± 9.7
CV Mid (cm <sup>3</sup> )	41.5 ± 12.4	15.4 ± 7.0
CV Apical (cm <sup>3</sup> )	25.4 ± 6.0	11.3 ± 3.9

Abbreviation: EF: Ejection fraction, CV: Chamber volume

**Commented [JK1]:** Changes to table 1 in regards to chamber diameters and volmes

**Deleted:** 3.9 ± 3.1

**Formatted:** Font: 8 pt

**Deleted:** 3.1 ± 2.8

**Formatted:** Font: 8 pt

**Formatted:** Font: 8 pt

**Deleted:** 3.7 ± 3.2

**Formatted:** Font: 8 pt

**Deleted:** 2.6 ± 2.9

**Formatted:** Font: 8 pt

**Deleted:** 2.7 ± 2.9

**Formatted:** Font: 8 pt

**Deleted:** 1.8 ± 1.9

**Deleted:** EV

**Deleted:** 47.4 ± 22.0

**Formatted:** Font: 8 pt

**Deleted:** 18.6 ± 10.9

**Formatted:** Font: 8 pt

**Deleted:** EV

**Formatted:** Font: 8 pt

**Deleted:** 42.2 ± 20.7

**Formatted:** Font: 8 pt

**Deleted:** 18.5 ± 8.6

**Deleted:** EV

**Formatted:** Font: 8 pt

**Deleted:** 23.1 ± 11.6

**Formatted:** Font: 8 pt

**Deleted:** 9.2 ± 4.8

**Deleted:** EV

**Deleted:** Ejection

The average age of the subjects was  $30.5 \pm 7.8$  years and body weight and body mass index (BMI) were  $149.3 \pm 34.7$  lbs and  $23.5 \pm 5.4$ , respectively. Monitored mean heart rate (HR) from all studies was  $66.6 \pm 8.0$  bpm while mean blood pressure (BP) was  $120.0 \pm 16.7/77.3 \pm 15.1$  mmHg. The full LV chamber quantifications are given in Table 1 and the strain-based contractile parameters in Table 2. The chamber quantities

**Table 2. Systolic and Diastolic Strains**

Strain	Diastolic	Systolic
$E_{cc}$ Basal	$-0.02 \pm 0.01$	$-0.15 \pm 0.04$
$E_{cc}$ Mid	$-0.03 \pm 0.01$	$-0.21 \pm 0.03$
$E_{cc}$ Apical	$-0.02 \pm 0.01$	$-0.20 \pm 0.03$
$E_{ll}$ Basal	$-0.04 \pm 0.01$	$-0.08 \pm 0.02$
$E_{ll}$ Mid	$-0.06 \pm 0.01$	$-0.12 \pm 0.03$
$E_{ll}$ Apical	$-0.10 \pm 0.02$	$-0.17 \pm 0.04$
$E_{rr}$ Basal	$0.11 \pm 0.01$	$0.27 \pm 0.03$
$E_{rr}$ Mid	$0.07 \pm 0.01$	$0.25 \pm 0.03$
$E_{rr}$ Apical	$0.06 \pm 0.01$	$0.25 \pm 0.02$
$E_{rc}$ Basal	$0.00 \pm 0.01$	$-0.02 \pm 0.01$
$E_{rc}$ Mid	$0.01 \pm 0.01$	$0.02 \pm 0.01$
$E_{rc}$ Apical	$0.02 \pm 0.01$	$0.03 \pm 0.01$
$E_{cl}$ Basal	$-0.01 \pm 0.01$	$-0.08 \pm 0.03$
$E_{cl}$ Mid	$0.00 \pm 0.00$	$0.00 \pm 0.01$
$E_{cl}$ Apical	$0.01 \pm 0.00$	$0.04 \pm 0.02$
$E_{cl}$ Basal	$0.02 \pm 0.00$	$0.05 \pm 0.02$
$E_{cl}$ Mid	$0.02 \pm 0.00$	$0.05 \pm 0.01$
$E_{cl}$ Apical ( $^{\circ}$ )	$0.00 \pm 0.00$	$0.02 \pm 0.01$
Rotation Basal ( $^{\circ}$ )	$-0.80 \pm 1.00$	$-5.50 \pm 2.89$
Rotation Mid ( $^{\circ}$ )	$2.40 \pm 0.94$	$8.20 \pm 2.91$
Rotation Apical ( $^{\circ}$ )	$4.90 \pm 1.57$	$18.10 \pm 4.59$
Torsion Basal ( $^{\circ}$ )	$2.50 \pm 0.52$	$9.20 \pm 1.94$
Torsion Mid ( $^{\circ}$ )	$2.00 \pm 0.43$	$8.30 \pm 1.84$

measured including wall thickness values of  $7.6 \pm 1.1$  mm in the apex,  $7.7 \pm 1.4$  mm at the mid-ventricle and  $7.6 \pm 1.5$  mm at the basal segment as well as other parameters such as CD, EDV, ESV and EF are comparable to values found in our semi-automated validation study and in others. Similar observations can be made regarding the strains given in Table 2 against those observed in our validation study and others [18, 19, 23, 26]. The values for shear strains in Table 2 that were critical for computations of torsion are also comparable to those found in previous literature; in particular  $E_{cl}$  values are very similar to the Young et al. study which reported 0.01-0.03 for apical, 0.03-0.04 for mid-ventricular, and 0.03-0.04 for basal regions [18, 27-30]. Figure 3 shows the 3D surface strain maps in the entire LV for radial, circumferential and longitudinal strains in a single healthy subject that contribute to the computation of the strain-based torsion (4). Bland Altman biases and limits of agreement for torsional comparisons between the validated semi-automated boundary contours given by (5) and the strain-based formula given by (4) were  $0.20 \pm 2.4^{\circ}$  and  $0.19 \pm 1.97^{\circ}$  for mid-ventricular and basal sub-regions, respectively (Figure 4). Furthermore, these cross-validated values are strongly comparable to values

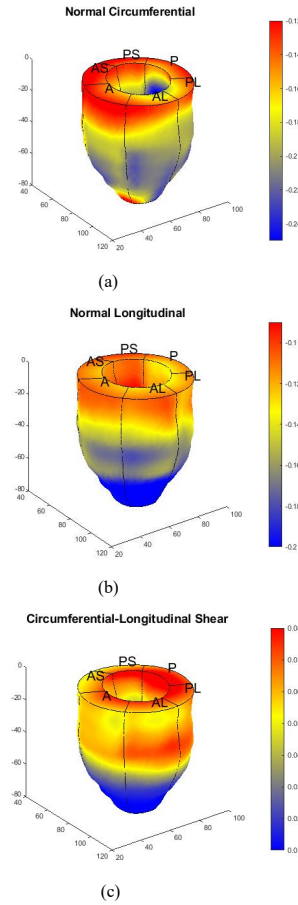


**Figure 3.** The three-dimensional strain tensor components that contribute towards strain-based computations of torsion. found in a multitude of literature [1, 23, 25]. Strong Pearson's correlations found between torsion and EF were  $R^2 = 0.80$  ( $p < 0.001$ ) for the mid-ventricular and  $R^2 = 0.82$  ( $p < 0.001$ ) for the basal segments. This strong correlation demonstrates the well-established phenomenon that both subendocardial and subepicardial shortening cause a relative rotation of the base (and mid-ventricle) in the clockwise direction and to the apex in counterclockwise and clockwise directions thus producing a torsional effect that drives ejection [1, 2].

This interaction between torsion and EF can also be observed from Figure 5 which shows peak torsions as coincidental with peak EF for all segments. Time taken

for automated 3D myocardial segmentation combined with strain analysis was  $6.7 \pm 3.0$  minutes per subject using the computational capability of a 3.4 GHz Intel Core processor, 16 GB of RAM and a 64-bit operating

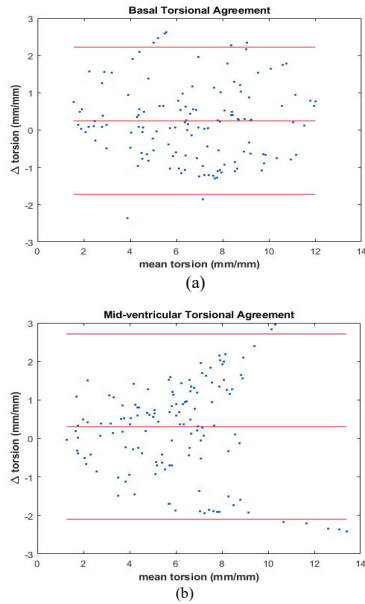


**Figure 4.** (a) Bland Altman agreement between two methods of torsion computations which are the strain-based and boundary-motion based methods conducted at the LV (a) basal and (b) mid-ventricular region.

system. The time taken for computing 3D RPIM strains was less than 15 seconds per timeframe, with approximately 15 partitions per subject, which resulted in total time taken for generating strains for the entire end-diastole to end-systole period to be  $2.2 \pm 0.9$  minutes.

#### IV. SUMMARY

In this paper, a fully automated methodology for comprehensively determining LV contractile parameters is presented, which was specifically developed to eliminate the pitfalls of operator error and reduce processing time (found to be approximately seven minutes for the duration of systolic ejection). This state-of-the-art algorithm is built on multi-threshold based quantization and phase unwrapping of complex DENSE images for computing chamber dimensions and contractile parameters such as LV cavity volumes, EF, mass, 3D strain tensors and others following isovolumetric contraction. It encompasses an existing

and validated methodology for semi-automatically determining LV chamber boundaries and normal strains during contraction. This study outlines enhancement of the semi-automated technique to include the analysis of 3D shear strains, twist and torsion that are vital towards understanding the mechanisms of isovolumetric contraction that drive ejection. In this regard Bland Altman analyses (with limits of agreement not exceeding  $2.5^\circ$ ) of the two torsion techniques provided cross-validation for the torsional computations. Furthermore, Pearson's correlations between EF and torsion demonstrate the capability to establish the interaction between these parameters and the viability of this procedure for use in examining healthy subjects.

Ultimately, we provide a unique and unprecedented

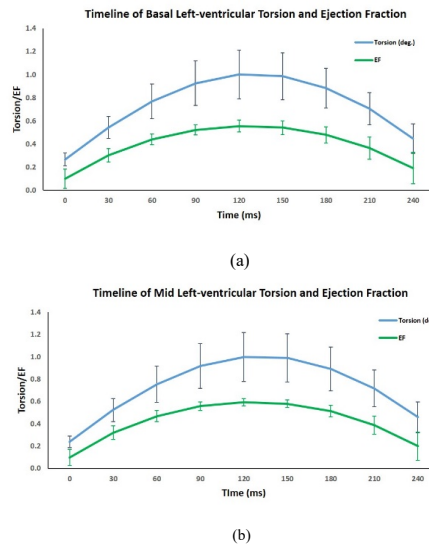


**Figure 5.** Timing of ventricular torsion whose mechanism drives ejection fraction, in the (a) basal and (b) mid-ventricular regions. Torsion values are normalized to maximum values of  $9.1^\circ$  and  $8.3^\circ$  at the base and mid-ventricle, respectively.

methodology for observing how subendocardial-to-subepicardial as well as apex-to-base rotations/torques related to myofiber function can be demonstrated via the correlation between torsion and EF. Our future goal is to establish if cardiac pathologies give rise to weakened trends in the relation between torsion and EF, in which case our methodology can become a powerful tool in diagnosing sub-clinical disease in conditions such as cardiomyopathies, ischemia and others.

#### ACKNOWLEDGMENTS

We are very appreciative of staff at the Imaging Center,

Children's and Women's Hospital, University of South Alabama in helping us acquire the MRI data. This study was funded by USAFDC Project: 144182 450500 4200.

#### REFERENCES

- [1] P. P. Sengupta, A. J. Tajik, K. Chandrasekaran, and B. K. Khandheria, "Twist mechanics of the left ventricle: principles and application," *JACC Cardiovasc Imaging*, vol. 1, no. 3, pp. 366-76, May 2008.
- [2] P. P. Sengupta, B. K. Khandheria, and J. Narula, "Twist and untwist mechanics of the left ventricle," *Heart Fail Clin*, vol. 4, no. 3, pp. 315-24, Jul 2008.
- [3] I. K. Russel, M. J. Gotte, J. G. Bronzwaer, P. Knaepen, W. J. Paulus, and A. C. van Rossum, "Left ventricular torsion: an expanding role in the analysis of myocardial dysfunction," *JACC Cardiovasc Imaging*, vol. 2, no. 5, pp. 648-55, May 2009.
- [4] Y. Notomi *et al.*, "Measurement of ventricular torsion by two-dimensional ultrasound speckle tracking imaging," *J Am Coll Cardiol*, vol. 45, no. 12, pp. 2034-41, Jun 21 2005.
- [5] D. Kim, W. D. Gilson, C. M. Kramer, and F. H. Epstein, "Myocardial tissue tracking with two-dimensional cine displacement-encoded MR imaging: development and initial evaluation," *Radiology*, vol. 230, no. 3, pp. 862-71, Mar 2004.
- [6] B. S. Spottiswoode *et al.*, "Tracking myocardial motion from cine DENSE images using spatiotemporal phase unwrapping and temporal fitting," *IEEE Trans Med Imaging*, vol. 26, no. 1, pp. 15-30, Jan 2007.
- [7] A. H. Aletras, S. Ding, R. S. Balaban, and H. Wen, "DENSE: displacement encoding with stimulated echoes in cardiac functional MRI," *J Magn Reson*, vol. 137, no. 1, pp. 247-52, Mar 1999.
- [8] X. Zhong *et al.*, "Comprehensive cardiovascular magnetic resonance of myocardial mechanics in mice using three-dimensional cine DENSE," *J Cardiovasc Magn Reson*, vol. 13, p. 83, Dec 30 2011.
- [9] X. Zhong, B. S. Spottiswoode, C. H. Meyer, C. M. Kramer, and F. H. Epstein, "Imaging three-dimensional myocardial mechanics using navigator-gated volumetric spiral cine DENSE MRI," *Magn Reson Med*, vol. 64, no. 4, pp. 1089-97, Oct 2010.
- [10] P. S. Liao, C. T. S., and P. C. Chung, "A Fast Algorithm for Multilevel Thresholding," *J. Inf. Sci. Eng.*, vol. 17, no. 5, pp. 713-727, 2001.
- [11] N. Otsu, "A Threshold Selection Method from Gray-Level Histograms," *IEEE Transactions on Systems, Man, and Cybernetics*, vol. 9, no. 1, pp. 62-66, 1979.
- [12] A. D. Gilliam and F. H. Epstein, "Automated motion estimation for 2-D cine DENSE MRI," *IEEE Trans Med Imaging*, vol. 31, no. 9, pp. 1669-81, Sep 2012.
- [13] B. S. Spottiswoode, X. Zhong, C. H. Lorenz, B. M. Mayosi, E. M. Meintjes, and F. H. Epstein, "Motion-guided segmentation for cine DENSE MRI," *Med Image Anal*, vol. 13, no. 1, pp. 105-15, Feb 2009.
- [14] J. Kar, A. K. Knutsen, B. P. Cupps, X. Zhong, and M. K. Pasque, "Three-dimensional regional strain computation method with displacement encoding with stimulated echoes (DENSE) in non-ischemic, non-valvular dilated cardiomyopathy patients and healthy subjects validated by tagged MRI," *J Magn Reson Imaging*, vol. 41, no. 2, pp. 386-96, Feb 2015.
- [15] E. O. Stejskal, "Use of spin echoes in a pulsed magnetic field gradient to study anisotropic, restricted diffusion and flow," *J. Chem. Phys.*, vol. 43, no. 10, pp. 3597-3603, 1965.
- [16] J. Kar, A. K. Knutsen, B. P. Cupps, and M. K. Pasque, "A validation of two-dimensional in vivo regional strain computed from displacement encoding with stimulated echoes (DENSE), in reference to tagged magnetic resonance imaging and studies in repeatability," *Ann Biomed Eng.*, vol. 42, no. 3, pp. 541-54, Mar 2014.
- [17] W. S. Cleveland and S. J. Devlin, "Locally-Weighted Regression: An Approach to Regression Analysis by Local Fitting," *Journal of the American Statistical Association*, vol. 83, no. 403, pp. 596-610, 1988.
- [18] J. Kar *et al.*, "Introduction to a mechanism for automated myocardium boundary detection with displacement encoding with stimulated echoes (DENSE)," *Br J Radiol*, p. 20170841, May 17 2018.
- [19] L. E. Hudsmith, S. E. Petersen, J. M. Francis, M. D. Robson, and S. Neubauer, "Normal human left and right ventricular and left atrial dimensions using steady state free precession magnetic resonance imaging," *J Cardiovasc Magn Reson*, vol. 7, no. 5, pp. 775-82, 2005.
- [20] G. R. Liu, *Meshfree Methods: Moving Beyond the Finite Element Method.*, 2 ed. Boca Raton: CRC Press, 2009, p. 792.
- [21] J. G. Wang and G. R. Liu, "A point interpolation meshless method based on radial basis functions," *Int J Numer Methods Eng* vol. 54, pp. 1623-1648, 2002.
- [22] J. G. Wang and G. R. Liu, "On the optimal shape parameters of radial basis functions used for 2-D meshless methods," *Computer Methods in Applied Mechanics and Engineering*, vol. 191, no. 23-24, pp. 2611-2630, 2002.
- [23] M. J. Gotte *et al.*, "Myocardial strain and torsion quantified by cardiovascular magnetic resonance tissue tagging: studies in normal and impaired left ventricular function," *J Am Coll Cardiol*, vol. 48, no. 10, pp. 2002-11, Nov 21 2006.
- [24] I. K. Russel *et al.*, "Increased left ventricular torsion in hypertrophic cardiomyopathy mutation carriers with normal wall thickness," *J Cardiovasc Magn Reson*, vol. 13, p. 3, Jan 10 2011.
- [25] I. K. Russel, S. R. Tecelao, J. P. Kuijter, R. M. Heethaar, and J. T. Marcus, "Comparison of 2D and 3D calculation of left ventricular torsion as circumferential-longitudinal shear angle using cardiovascular magnetic resonance tagging," *J Cardiovasc Magn Reson*, vol. 11, p. 8, Apr 20 2009.
- [26] K. Alfakih, S. Plein, H. Thiele, T. Jones, J. P. Ridgway, and M. U. Sivananthan, "Normal human left and right ventricular dimensions for MRI as assessed by turbo gradient echo and steady-state free precession imaging sequences," *J Magn Reson Imaging*, vol. 17, no. 3, pp. 323-9, Mar 2003.
- [27] A. A. Young, C. M. Kramer, V. A. Ferrari, L. Axel, and N. Reichek, "Three-dimensional left ventricular deformation in hypertrophic cardiomyopathy," *Circulation*, vol. 90, no. 2, pp. 854-67, Aug 1994.
- [28] C. C. Moore, C. H. Lugo-Olivieri, E. R. McVeigh, and E. A. Zerhouni, "Three-dimensional systolic strain patterns in the normal human left ventricle: characterization with tagged MR imaging," *Radiology*, vol. 214, no. 2, pp. 453-66, Feb 2000.
- [29] A. T. Hess, X. Zhong, B. S. Spottiswoode, F. H. Epstein, and E. M. Meintjes, "Myocardial 3D strain calculation by combining cine displacement encoding with stimulated echoes (DENSE) and cine strain encoding (SENC) imaging," *Magn Reson Med*, vol. 62, no. 1, pp. 77-84, Jul 2009.
- [30] J. Kar *et al.*, "Preliminary investigation of multiparametric strain Z-score (MPZS) computation using displacement encoding with simulated echoes (DENSE) and radial point interpretation method (RPIM)," *J Magn Reson Imaging*, vol. 44, no. 4, pp. 993-1002, Oct 2016.